INORGANIC CHEMISTRY
FRONTIERS

RESEARCH ARTICLE

View Article Online
View Journal | View Issue

Cite this: *Inorg. Chem. Front.*, 2023, **10**, 1328

From $AgTeO_2F$ and $Ag_2(TeO_2F_2)$ to $Ag_3F_3(TeF_6)(TeO_2)_{12}$: the first silver tellurite oxyfluorides with linear and nonlinear optical properties†

Bo Zhang,[a,b,c] Jia-Hang Wu,[a,b] Chun-Li Hu,[a] Ya-Feng Li,[b] Fang Kong *[a,c] and Jiang-Gao Mao *[a,c]

Received 24th October 2022,
Accepted 2nd January 2023

DOI: 10.1039/d2qi02272a

rsc.li/frontiers-inorganic

The first examples of silver fluorotellurites, namely, $AgTeO_2F$ and $Ag_2(TeO_2F_2)$, and the first silver fluoride tellurite, $Ag_3F_3(TeF_6)(TeO_2)_{12}$, have been obtained successfully under mild hydrothermal conditions. $AgTeO_2F$ displays a new 2D structure composed of a 2D silver oxide layer strengthened by 1D $[TeO_2F]_\infty$ chains. $Ag_2(TeO_2F_2)$ exhibits a new 3D construction consisting of a 3D silver oxyfluoride framework with 1D polyhedral ring channels occupied by the isolated TeO_2F_2 groups. $Ag_3F_3(TeF_6)(TeO_2)_{12}$ features the first 3D neutral $[TeO_2]_\infty$ open framework with 8- and 4-MPR channels along the *a*-, *b*- and *c*-axes. $AgTeO_2F$ and $Ag_2(TeO_2F_2)$ crystallize in the centrosymmetric space group while $Ag_3F_3(TeF_6)(TeO_2)_{12}$ is in a non-centrosymmetric space group. $Ag_3F_3(TeF_6)(TeO_2)_{12}$ shows a unique nonlinear optical property with an SHG intensity of about 70% that of commercial KH_2PO_4, while $AgTeO_2F$ and $Ag_2(TeO_2F_2)$ present an apparent linear optical property and their birefringence is calculated as 0.078 and 0.032@1064 nm, respectively. This work further confirms that fluorination in tellurium(IV) oxides can greatly enrich the structural chemistry and optical properties of metal tellurites.

Introduction

Second harmonic generation (SHG) materials have continued to be in great demand due to their capacity of laser frequency conversion, material micromachining, photolithography and so on.[1–9] The first requirement for an SHG material is a non-centrosymmetric (NCS) structure since it is a physical quantity described by an odd-order tensor.[10–14] The lone pair cation of Te(IV), with a $5s^2$ electronic configuration, can exhibit three different kinds of asymmetric coordination mode, namely, TeO_3 trigonal pyramid, TeO_4 seesaw-like group, and TeO_5 tetragonal pyramid, when it coordinates with oxygen ligands due to the hybridization between the s- and p-orbitals of the cation and anions.[15] These polar tellurite groups can stimulate the formation of NCS structures, making metal tellurites good candidates for SHG materials.[16–20] Metal tellurites can also display plentiful structure types because the polar oxyanions can join together by condensation to generate 0D clusters,[21–23] 1D chains,[24–27] 2D layers[28,29] and even 3D frameworks.[30,31]

Fluorine, as the most electronegative element, could replace oxygen ligands due to their similar ionic radii.[32–34] When fluorine atoms are introduced into oxide compounds, fluoride compounds often can display excellent comprehensive performance and abundant structure types,[35–38] such as $RbTeMo_2O_8F$ (27 × KDP, 3.63 eV),[39] $Ba(MoO_2F)_2(TeO_3)_2$ (7.8 × KDP, 2.96 eV),[40] and $BaF_2TeF_2(OH)_2$ (3 × KDP, 5.9 eV)[41] in metal tellurites. Fluorine-containing tellurite compounds (or tellurite oxyfluorides) can be classified into fluoride tellurites and fluorotellurites according to the connection mode of the fluorine element. In fluorotellurites, the fluorine atoms are connected with the lone pair cation of Te(IV); in other words, there are Te(IV)–F bonds in the structures, such as $Bi_3F(TeO_3)(TeO_2F_2)_3$[42] and $HgTeO_2F(OH)$.[43] $BaF_2TeF_2(OH)_2$ is the first reported SHG material in metal fluorotellurites, which has proved to be a promising UV nonlinear optical material.[41] The Te–F bonds in $BaF_2TeF_2(OH)_2$ play an important role in the wide band gap. In fluoride tellurites, there are no Te(IV)–F bonds, and the fluorine atoms are linked with the other cations, such as d^0 transition metals (TM), $RbTeMo_2O_8F$[39] and $Ba(MoO_2F)_2(TeO_3)_2$,[40] and alkali metals, $Li_7(TeO_3)_3F$.[44] $RbTeMo_2O_8F$ containing a MoO_5F octahedron features the strongest SHG material of metal tellurites at both the visible

[a]*State Key Laboratory of Structural Chemistry, Fujian Institute of Research on the Structure of Matter, Chinese Academy of Sciences, Fuzhou 350002, P. R. China. E-mail: kongfang@fjirsm.ac.cn, mjg@fjirsm.ac.cn*
[b]*College of Chemistry, Fuzhou University, Fuzhou 350108, P. R. China*
[c]*University of Chinese Academy of Sciences, Beijing 100049, P. R. China*

†Electronic supplementary information (ESI) available: Crystallographic data, important bond distances and angles, simulated and measured PXRD patterns, infrared spectra, and computational method. CCDC 2214235–2214237. For ESI and crystallographic data in CIF or other electronic format see DOI: https://doi.org/10.1039/d2qi02272a

and near-infrared ranges, and the MoO_5F octahedron contributed the most to the SHG efficiency of $RbTeMo_2O_8F$. Therefore, fluorination in tellurites not only broadens the band gap of metal tellurites, but can also increase the SHG intensity of crystals. However, compared with tellurite oxides, tellurite oxyfluorides, including fluoride tellurites and fluorotellurites, are still rare due to their synthetic difficulty. It is still very necessary to enrich the structural chemistry and the SHG crystal types in metal tellurite oxyfluorides.

To increase the success rate of NCS structures, the d^{10} TM cation Ag^+ was chosen to balance the charge due to its large polar displacement.[28,45–48] After an extensive survey, we found that no silver tellurites with the fluorine element have been reported yet. Our efforts in the silver–tellurite–fluorine system successfully result in the first examples of silver fluorotellurites and the first silver fluoride tellurite, namely, $AgTeO_2F$ and $Ag_2(TeO_2F_2)$, and $Ag_3F_3(TeF_6)$ $(TeO_2)_{12}$. Among these compounds, $Ag_3F_3(TeF_6)$ $(TeO_2)_{12}$ crystallized in an NCS space group and presented a moderate SHG response of 0.7 × KH_2PO_4 (KDP) at 1064 nm. Herein, we report their syntheses, crystal structures, and thermal and optical properties from theoretical and experimental aspects.

Experimental section

Reagents

Silver fluoride (AgF, 98+%, AR), tellurium dioxide (TeO_2, 99.9%, AR) and hydrofluoric acid (HF, 40+%, AR) were obtained commercially and used as received. Caution! Hydrofluoric acid is toxic and corrosive! It must be handled with extreme caution and with the appropriate protective equipment and training.

Syntheses

The three compounds were successfully synthesized *via* a mild hydrothermal method based on the following chemical proportions: AgF (0.127 g, 1.0 mmol), TeO_2 (0.160 g, 1.0 mmol), hydrofluoric acid (0.25 mL) and 1 mL of deionized water for $AgTeO_2F$; AgF (0.127 g, 1.0 mmol), TeO_2 (0.080 g, 0.5 mmol), hydrofluoric acid (0.25 mL) and 1.5 mL of deionized water for $Ag_2(TeO_2F_2)$; AgF (0.102 g, 0.8 mmol), TeO_2 (0.256 g, 1.6 mmol), hydrofluoric acid (0.25 mL) and 0.5 mL of deionized water for $Ag_3F_3(TeF_6)(TeO_2)_{12}$. It is worth noting that the amount of deionized water is critical in these reactions besides the proportions of the raw materials. The mixtures were placed in a 23 mL Teflon liner equipped with a stainless-steel autoclave. These samples were heated to 220 °C, maintained for 48 h, and then cooled to 30 °C at 2.3 °C h^{-1}. After washing with deionized water, the products were dried in air at room temperature. As shown in Fig. S1,† the three compounds exhibit three different morphologies: lamellar $AgTeO_2F$, columnar $Ag_2(TeO_2F_2)$ and octahedral $Ag_3F_3(TeF_6)(TeO_2)_{12}$, and the three kinds of crystals were obtained in yields of about 58%, 43% and 75% (based on Te), respectively. The existence and distribution of Ag, Te and F were demonstrated *via* the elemental distribution maps (Fig. 1). As shown in Fig. S2,† the experimental powder X-ray diffraction (PXRD) patterns are in good agreement with the calculated ones, so their purities are certified.

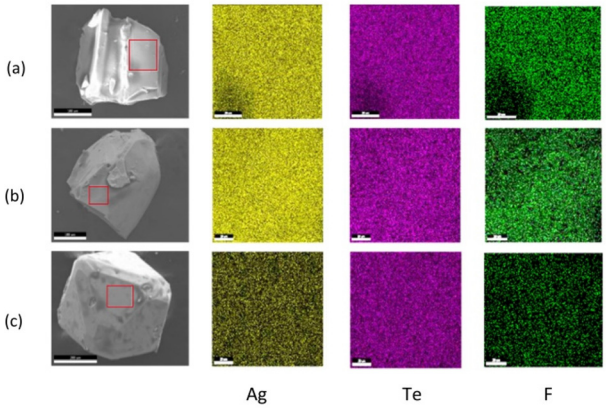

Fig. 1 SEM images of $AgTeO_2F$ (a), $Ag_2(TeO_2F_2)$ (b) and $Ag_3F_3(TeF_6)$ $(TeO_2)_{12}$ (c) and their elemental distribution maps.

Single-crystal structure determination

Single-crystal X-ray diffraction data of $AgTeO_2F$, $Ag_2(TeO_2F_2)$ and $Ag_3F_3(TeF_6)$ $(TeO_2)_{12}$ were collected on an Agilent Technologies SuperNova dual-wavelength CCD diffractometer with graphite-monochromated Mo Kα radiation (λ = 0.71073 Å) at room temperature. Cell refinement and data reduction were conducted with CrysAlisPro and absorption correction based on the multi-scan method was applied.[49] The structures were determined by direct methods and refined by full-matrix least-squares fitting on F^2 using the SHELXL-2017 software package.[50] The atoms were refined with anisotropic thermal parameters. The detailed crystallographic data of the three structures are listed in Table 1, and some selected atomic coordinates, bond lengths and angles are listed in Tables S1–S3.† Detailed information on the crystal structure of the three compounds can be obtained from the Cambridge Crystallographic Data Center.

Powder X-ray diffraction

Powder X-ray diffraction (PXRD) data of the three crystals were recorded on a Rigaku Miniflex600 diffractometer equipped with graphite-monochromated Cu Kα radiation at room temperature. The 2θ range is set to 5–70°, and the scan step size is 0.02°.

Energy-dispersive X-ray spectroscopy

Microprobe elemental analysis was conducted with the aid of a field-emission scanning electron microscope (JSM6700F) outfitted with an energy-dispersive X-ray spectroscope (Oxford INCA).

Table 1 Summary of crystal data and structural refinements for $AgTeO_2F$, $Ag_2(TeO_2F_2)$ and $Ag_3F_3(TeF_6)(TeO_2)_{12}$

Molecular formula	$AgTeO_2F$	$Ag_2(TeO_2F_2)$	$Ag_3F_3(TeF_6)(TeO_2)_{12}$
Formula weight	286.47	413.34	2575.07
Crystal system	Monoclinic	Orthorhombic	Cubic
Space group	$P2_1/c$	$Pbca$	$P\bar{4}3n$
Temperature (K)	292.38(10)	293.39(10)	294.15
$F(000)$	728	2880	2245
a/Å	8.7523(14)	15.6642(13)	11.3998(5)
b/Å	6.3759(9)	6.8862(5)	11.3998(5)
c/Å	5.4505(8)	16.5328(12)	11.3998(5)
α (°)	90	90	90
β (°)	91.396(14)	90	90
γ (°)	90	90	90
V/Å^3	304.07(8)	1783.3(2)	1481.47(19)
Z	4	16	2
D_c (g cm^{-3})	6.258	6.158	5.773
GOF on F^2	1.008	1.073	1.138
Flack factor	—	—	0.48(9)
R_1, wR_2 [$I > 2\sigma(I)$]^a	0.0223, 0.0439	0.0306, 0.0704	0.0200, 0.0434
R_1, wR_2 (all data)^a	0.0267, 0.0462	0.0377, 0.0750	0.0251, 0.0460

^{a} $R_1 = \sum||F_o| - |F_c||/\sum|F_o|$, $wR_2 = \{\sum w[(F_o)^2 - (F_c)^2]^2/\sum w[(F_o)^2]^2\}^{1/2}$.

Spectroscopic measurements

The IR spectrum was recorded using a Magna 750 FT-IR spectrometer under an air background, and the selected range is 4000–400 cm^{-1}. The UV-vis-NIR diffuse reflection spectrum was measured using a PerkinElmer Lambda 950 UV-vis-NIR spectrophotometer with a $BaSO_4$ powder board as a reference for 100% reflectance, and the recording range was 200–2000 nm. Absorption data were calculated from the diffuse reflection data by the Kubelka–Munk function: $\alpha/S = (1 - R)^2/2R$, in which α and S represent the absorption coefficient and the scattering coefficient, respectively. The band gap value can be given by extrapolating the absorption edge to the baseline in the α/S *versus* energy graph.

Thermal analysis

A NETZCH STA 449F3 thermal analyzer was used to analyze the thermal stability of the three crystals. The three samples were heated in alumina crucibles from 20 °C to 1000 °C under nitrogen gas at a rate of 15 °C min^{-1}.

SHG measurements

Powder SHG measurements were carried out using a modified method of Kurtz and Perry. An irradiation laser beam (λ = 1.064 μm) is generated with a Nd:YAG solid-state laser equipped with a Kurtz and Perry setup.[51] The SHG signal oscilloscope traces of the $Ag_3F_3(TeF_6)(TeO_2)_{12}$ and KDP samples in a particle size range (150–210 μm) were both recorded.

Results and discussion

Structure of $AgTeO_2F$

Equivalent silver and tellurium sources resulted in the production of $AgTeO_2F$. $AgTeO_2F$ crystallizes in the monoclinic space group $P21/c$. Its asymmetric unit contains 1 Ag, 1 Te, 2 O and 1 F atoms (Table S1†). The Ag(1) atom is 4-coordinated into a distorted tetrahedron AgO_4 with the lengths of Ag–O bonds ranging from 2.319(4) to 2.478(5) Å. The Te(1) atom connects with 3 O and 1 F atoms, forming a polar TeO_3F group in a seesaw-like configuration. The Te–O bond distances are in the range of 1.832(4)–2.162(4) Å and the Te–F bond length is 2.029(4) Å, which are consistent with the reported metal tellurites.[43,52–57] The calculated total bond valences for Ag and Te are 0.825 and 4.031, indicating their oxidation states of +1 and +4 respectively (Table S2†).

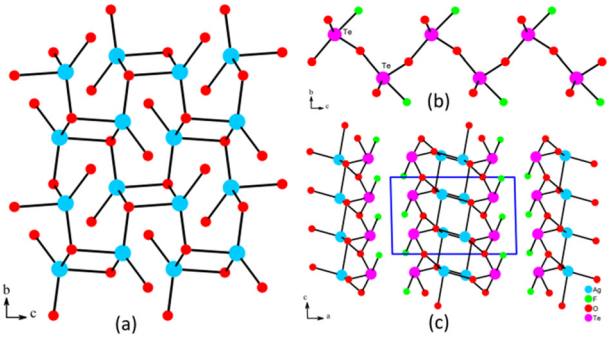

Fig. 2 Silver oxide layer in the *bc* plane (a), the 1D chain of Te–O–F (b), and the layer structure of $AgTeO_2F$ (c).

$AgTeO_2F$ presents a new 2D layered structure. Within the structure, the AgO_4 tetrahedra were corner- and edge-shared into a silver oxide layer parallel to the *bc* plane (Fig. 2a). The TeO_3F groups were corner-shared into a zigzag chain along the *c*-axis (Fig. 2b). The fluorotellurite 1D chains were linked on the both sides of the silver oxygen layers *via* Te–O–Ag bonds, forming the 2D layered structure of $AgTeO_2F$ (Fig. 2c). The lone pairs of tellurites were pointed to the space between layers. The interlayer distance was calculated as 8.75 Å.

Structure of $Ag_2(TeO_2F_2)$

When we increased the ratio of silver, a new compound of $Ag_2(TeO_2F_2)$ was achieved. $Ag_2(TeO_2F_2)$ presents a new 3D construction composed of a 3D silver oxygen framework strengthened by TeO_2F_2 units. The structure crystallized in the orthorhombic space group *Pbca*. Its asymmetric unit includes 4 Ag, 2 Te, 4 O and 2 F atoms. Both of the Te(IV) cations were four-coordinated in seesaw-like TeO_2F_2 groups with the Te–O and Te–F bonds in the ranges of 1.848–1.869 Å and 2.021–2.068 Å, respectively (Fig. S3a and S3b†). The four Ag^+ cations were connected with both O and F atoms, forming $Ag(1)O_3F$, $Ag(2)O_3F_2$, $Ag(3)O_4F$, and $Ag(4)O_3F$ polyhedra, respectively. The Ag–O and Ag–F bond distances were in the ranges of 2.19(6)–2.663(8) and 2.458(6)–2.68(6) Å, respectively. The oxidation states of the Ag and Te atoms were proved to be +1 and +4, respectively. The calculated total bond valences for Ag(1), Ag(2), Ag(3), Ag(4), Te(1) and Te(2) are 0.769, 0.961, 0.711, 0.809, 4.007, and 4.066, respectively.

The $Ag(1)O_3F$ polyhedra were corner-shared in a Ag(1) chain along the *b*-axis, so were the Ag(2) polyhedra (Fig. 3a and b).

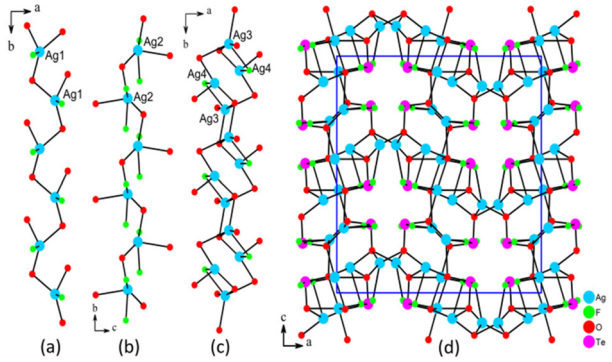

Fig. 3 Ag(1)–O–F zigzag chain (a), Ag(2)–O–F wave chain (b), 1D Ag(3)–Ag(4)–O–F chains (c), and 3D structure of $Ag_2(TeO_2F_2)$ (d).

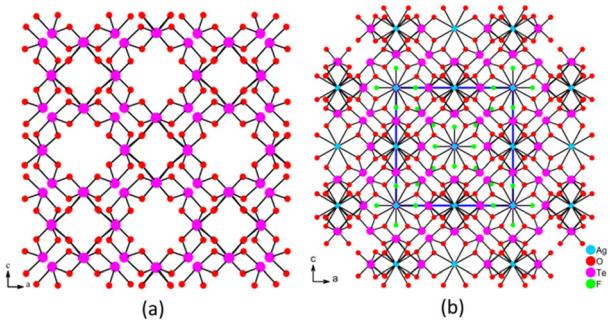

Fig. 4 The 3D skeleton with two different 1D channels (a), and the structure chart of AgO_8 and TeF_6 residing in the centre of 8-MPRs and 4-MPRs (b).

The $Ag(3)O_4F$ and $Ag(4)O_3F$ polyhedra were corner- and edge-shared into a 1D Ag(3)Ag(4) chain along the *b*-axis with four-member polyhedral rings (MPRs) (Fig. 3c). The Ag(3)Ag(4) chains were connected by the Ag(1) chain to form a 2D layer parallel with the *ab* plane (Fig. S3c†), which were further linked by the Ag(2) chains to a 3D silver oxyfluoride open framework with 1D 18-MPR channels along the *b*-axis (Fig. S3d†). The isolated $Te(1)O_2F_2$ and $Te(2)O_2F_2$ units were filled in the 18-MPR channels to strengthen the 3D structure of $Ag_2(TeO_2F_2)$ (Fig. 3d). Due to the blocking effect of TeO_2F_2 groups, the 18-MPR channels have been shrunk to 10-MPR channels with the lone pairs of tellurites pointed to the center of them.

Structure of $Ag_3F_3(TeF_6)(TeO_2)_{12}$

A mixed valence tellurium compound of $Ag_3F_3(Te^{VI}F_6)(Te^{IV}O_2)_{12}$ was obtained when we adjusted the reaction conditions further. $Ag_3F_3(TeF_6)(TeO_2)_{12}$ is crystallized in the cubic space group $P\bar{4}3n$. There are 1 Ag, 2 Te, 2 O and 2 F atoms in the asymmetric unit. Tetravalent Te(1) is coordinated with four O^{2-} anions into a TeO_4 quadrangular pyramid with the Te–O bond lengths ranging from 1.827(4) to 2.107(5) Å while the hexavalent Te(2) atom connects with 6 F atoms to form a TeF_6 octahedron with a Te–F bond length of 1.906(17) Å (Fig. S4a†). The Ag^+ cation is 8-coordinated into AgO_8 polyhedra with the length of Ag–O bonds ranging from 2.589(7) to 2.559(7) Å (Fig. S4b†). The oxidation state of Ag, Te(1) and Te(2) atoms was proved to be +1, +4 and +6, respectively, based on the calculated total bond valences of 1.000, 4.078 and 6.180 for Ag, Te(1) and Te(2), respectively.

$Ag_3F_3(TeF_6)(TeO_2)_{12}$ features an interesting 3D structure formed by the 3D $Ag_3F_3(TeO_2)_{12}$ framework embedded with the isolated (TeF_6) octahedra. The tetravalent $Te(1)O_4$ units were interconnected into a 3D neutral $[TeO_2]_\infty$ open framework by corner-sharing with 8- and 4-MPR channels along the *a*-, *b*- and *c*-axes (Fig. 4a). The Ag(1) cations were located in the two different 1D channels to form the 3D cationic framework of $[Ag_3(TeO_2)_{12}]^{3+}$ (Fig. S4c†). Interestingly, the silver cations were situated at the sites with symmetry of 222, namely, the twelve axis-center and the six face-center of the unit cell. The body center of the cubic structure was empty, and was filled by the isolated F(2) atoms and the (TeF_6) octahedron to balance the charge and support the framework, respectively (Fig. 4b). So, the structure of $Ag_3F_3(TeF_6)(TeO_2)_{12}$ can be described as a 3D construction composed of a 3D $Ag_3F_3(TeO_2)_{12}$ framework embedded with the neutral (TeF_6) octahedra.

From the elucidation of the structures, we can find that the quantity and site of the fluorine element are totally different in the three tellurite oxyfluorides. In $AgTeO_2F$, only one oxygen was replaced in the TeO_3F groups while two oxygen atoms were substituted in TeO_2F_2 of $Ag_2(TeO_2F_2)$. Only the Te(VI) groups were fluoride in $Ag_3F_3(TeF_6)(TeO_2)_{12}$. We think that the difference should be caused by the different synthesis conditions, especially from the molar ratio of AgF to TeO_2. When the ratio of AgF/TeO_2 was 1/1, $AgTeO_2F$ was obtained, of which the tellurite was a mono-substituted TeO_3F group. If the ratio was increased to 2/1, $Ag_2(TeO_2F_2)$ was isolated and disubstituted TeO_2F_2 groups were found. When the ratio was decreased to 1/2 and the content of solvent water was halved, partial Te(IV) oxidized into Te(VI) and mixed valence $Ag_3F_3(TeF_6)(TeO_2)_{12}$ was achieved. In the structure of $Ag_3F_3(TeF_6)(TeO_2)_{12}$, only Te(VI) groups were fluoride, which can be explained by the Hard–Soft–Acid–Base (HSAB) theory. Compared with a Te(IV) ion, Te(VI) has higher charge and a smaller radius, so it has stronger acidity. The fluorine element with strong electronegativity can be regarded as a hard base, which is liable to coordinate with cations with strong acidity. This work revealed that the fluorination in tellurium(IV) oxides can enrich the structural chemistry of metal tellurites greatly.

Thermal analyses

Thermogravimetric analyses (TGA) were performed to explore the thermal behavior of the three compounds. From Fig. 5a we can find that there are slight weight losses of about 0.94% and 0.97% in the ranges of 294–494 °C and 271–509 °C for $AgTeO_2F$ and $Ag_2(TeO_2F_2)$, respectively, corresponding to the escape of partial F_2 molecules. We checked the thermal stability of $AgTeO_2F$ and $Ag_2(TeO_2F_2)$ at 20, 300, 400 and 500 °C, respectively, by PXRD measurements. From the results shown in Fig. S5,† we can find that the PXRD patterns of the two

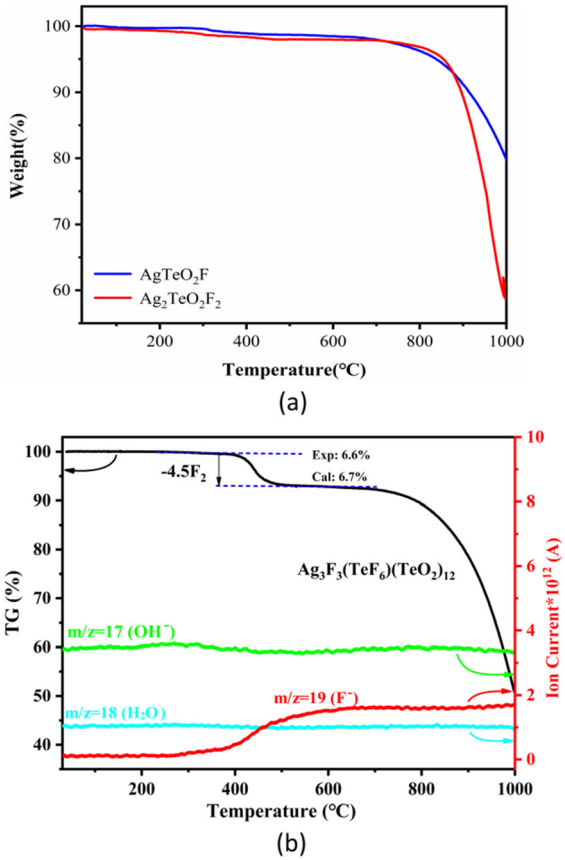

Fig. 5 TGA curves of $AgTeO_2F$ and $Ag_2(TeO_2F_2)$ (a), and the TG-MS curves of $Ag_3F_3(TeF_6)(TeO_2)_{12}$ (b).

samples at 300 °C could not match the patterns at room temperature, which indicates that the two crystals have been decomposed at 300 °C. The release of the TeO_2 molecule occurred at about 662 °C and 689 °C for $AgTeO_2F$ and $Ag_2(TeO_2F_2)$, respectively. The thermogravimetric-mass spectrometry (TG-MS) measurement was performed for $Ag_3F_3(TeF_6)(TeO_2)_{12}$ (Fig. 5b). The TG curve of $Ag_3F_3(TeF_6)(TeO_2)_{12}$ involves two steps of weight-losses. The first one (exp. 6.6%) in the range of 328 to 524 °C is consistent with the release of 4.5 F_2 molecules (cal. 6.7%). The second weight loss that occurred above 684 °C can be attributed to the evaporation of the TeO_2 molecules, which did not complete even at 1000 °C, just like the situations in $AgTeO_2F$ and $Ag_2(TeO_2F_2)$. The ion current curves of $Ag_3F_3(TeF_6)(TeO_2)_{12}$ indicate the existence of the fluorine element and the absence of the OH^- group or the H_2O molecule, which further proved the correctness of the formula.

IR and UV-vis-NIR spectra

The IR spectra revealed that no obvious absorption was found in the region 4000–800 cm^{-1} for the three compounds, indicating no hydroxy bonds in the structures (Fig. S5†). Their vibration bands were focused over the range of 400–780 cm^{-1}, which can be attributed to the Te–O and Te–F vibrations. These assignments correspond to the reported tellurites.[52,58–63]

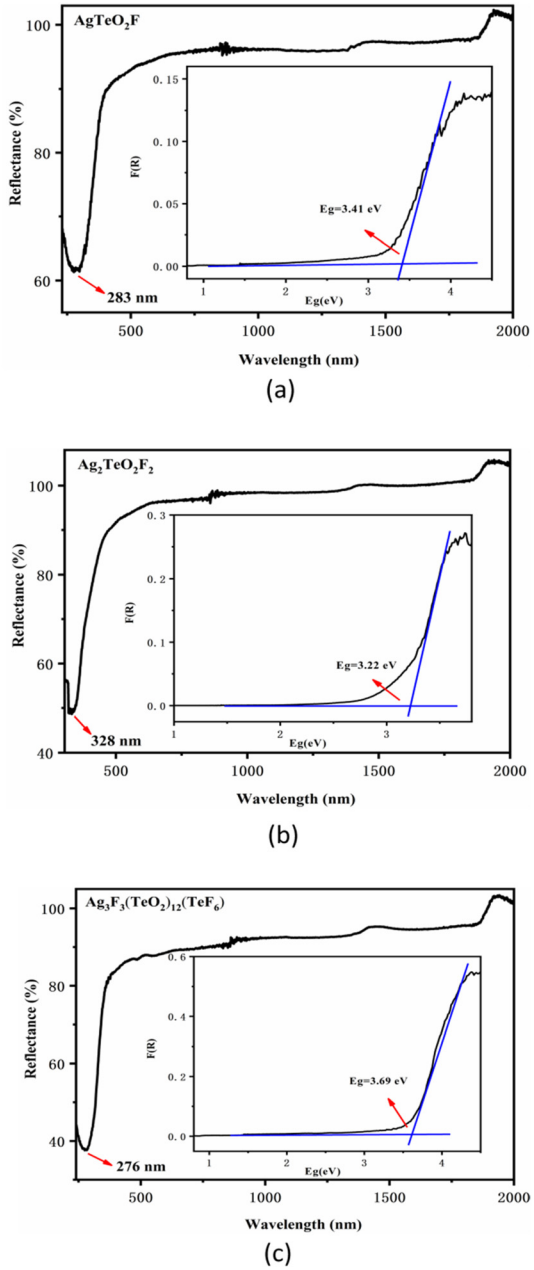

Fig. 6 UV-vis-NIR diffuse reflectance spectra of $AgTeO_2F$ (a), $Ag_2(TeO_2F_2)$ (b) and $Ag_3F_3(TeF_6)(TeO_2)_{12}$ (c).

The UV-vis-NIR diffuse-reflectance spectra of the three compounds show that they have no obvious absorption in the range of 500–2000 nm (Fig. 6). The ultraviolet absorption cutoff edges of $AgTeO_2F$, $Ag_2(TeO_2F_2)$ and $Ag_3F_3(TeF_6)(TeO_2)_{12}$ were 283, 328 and 276 nm, respectively, and their optical band gaps were measured as 3.41, 3.22 and 3.69 eV, respectively.

SHG measurements

For $Ag_3F_3(TeF_6)(TeO_2)_{12}$, measurement of the powder frequency-doubling effect was carried out by the method of Kurtz and Perry, employing a Q-switched Nd:YAG laser under

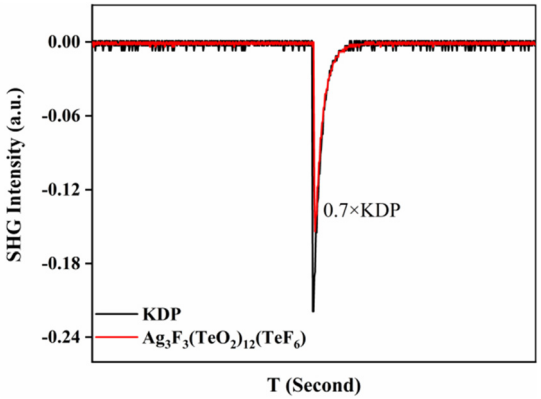

Fig. 7 The oscilloscope traces of the SHG signals for the samples (150–210 μm) of $Ag_3F_3(TeF_6)(TeO_2)_{12}$ and KDP under laser irradiation at 1064 nm.

1064 nm radiation. A sieved sample (70–100 mesh) was used to assess its second-order susceptibility coefficient. Powder SHG examination revealed that $Ag_3F_3(TeF_6)(TeO_2)_{12}$ displayed a moderate frequency-doubling efficiency of about 0.7 × KDP (Fig. 7).

Theoretical calculation

To access the birefringence of $AgTeO_2F$ and $Ag_2(TeO_2F_2)$, their linear optical properties have been studied using CASTEP based on DFT methods. Such work has not been performed for $Ag_3F_3(TeF_6)(TeO_2)_{12}$ due to its isotropic nature.

Fig. 8 presents the band structures along the high symmetry points of the first Brillouin zone for $AgTeO_2F$ and $Ag_2(TeO_2F_2)$. The state energies of the CBs and highest VBs of the two structures are shown in Table S4.† For $AgTeO_2F$, the maximum of VBs is situated at the Z point and the minimum of CBs is placed at the G point with a band gap of 2.29 eV, indicating that it is an indirect band gap compound (Fig. 8a). For $Ag_2(TeO_2F_2)$, the top of the VBs is located at the X point while the bottom of CBs is placed at the G point with a band gap of 1.64 eV, which shows that it also is an indirect band gap material (Fig. 8b). The calculated band gaps are much smaller than the experimental results, which was caused by the discontinuity of the exchange–correlation functional.[64] Therefore, scissor operators are 1.12 eV and 1.58 eV for $AgTeO_2F$ and $Ag_2(TeO_2F_2)$, respectively, which are used in the following optical property calculations.

The total and partial density of states are displayed in Fig. 9. The TDOS and PDOS of the two structures are very similar. In $AgTeO_2F$ and $Ag_2(TeO_2F_2)$, the VBs in the lower energy from −20 to −17 eV mostly originate from O 2s and Te

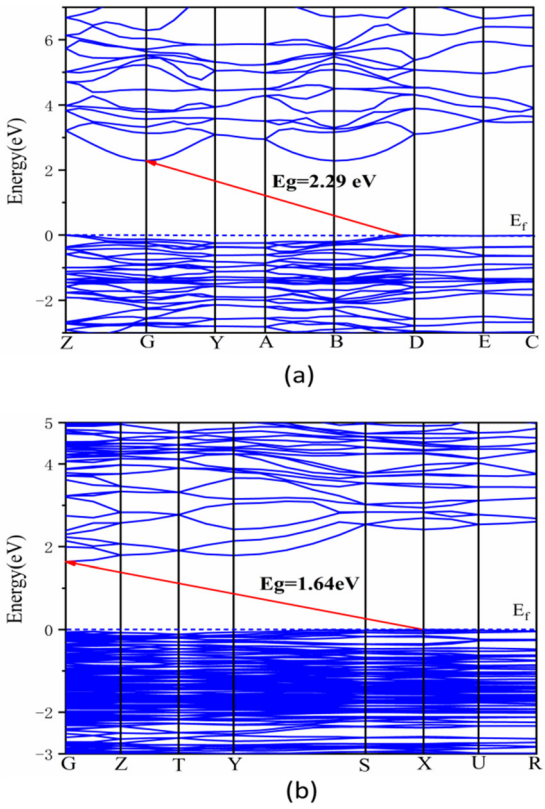

Fig. 8 Calculated band structures of $AgTeO_2F$ (a) and $Ag_2(TeO_2F_2)$ (b).

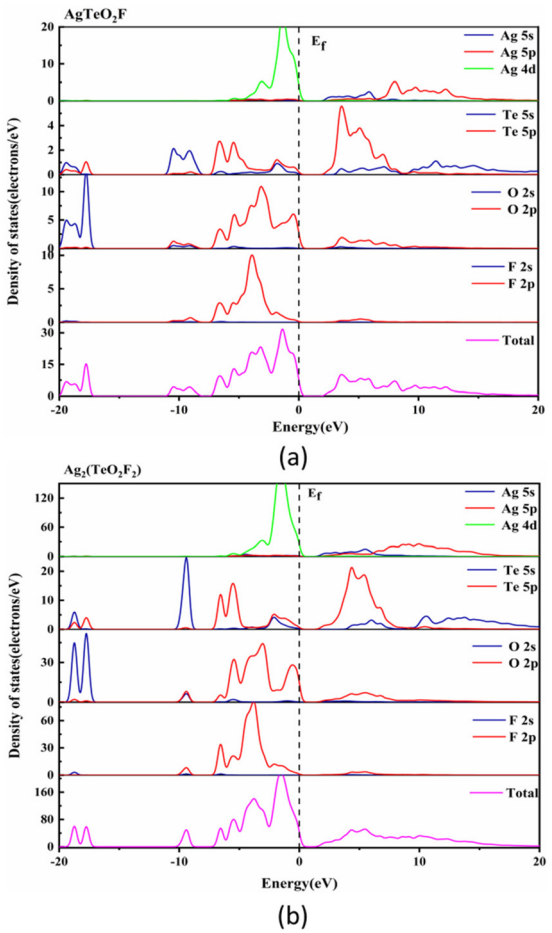

Fig. 9 The total and partial density of states for $AgTeO_2F$ (a) and $Ag_2(TeO_2F_2)$ (b).

5s5p. The CBs in the higher energy between 3.0 and 10.0 eV are composed of Te 5s5p and O 2p states primarily. To assign the electronic bands explicitly, we have concentrated our attention on the top of VBs and the bottom of CBs close to the Fermi level, which are able to clarify the majority of the bonding character. In $AgTeO_2F$ and $Ag_2(TeO_2F_2)$, we can find that the O-2p states and F-2p states match well with the states of Te-5p, which indicates the strong Te–O and Te–F bonding interactions. For $AgTeO_2F$ and $Ag_2(TeO_2F_2)$, the maximum of valence bands are mainly from the O-2p and Ag-4d non-bonded states, while the minimum of valence bands come from the empty Te-5p and Ag-5s orbitals primarily (Fig. 9). Therefore, the band gaps of $AgTeO_2F$ and $Ag_2(TeO_2F_2)$ are determined by O, Ag and Te atoms.

The linear optical response properties were calculated by the complex dielectric function $\varepsilon(\omega) = \varepsilon_1(\omega) + i\varepsilon_2(\omega)$. The dispersion curves of refractive indices based on the formula $n^2(\omega) = \varepsilon(\omega)$ displayed strong anisotropy. The frequency-dependent refractive indices for $AgTeO_2F$ and $Ag_2(TeO_2F_2)$ are shown in Fig. 10. For $AgTeO_2F$, the refractive indices follow the order of $n_{010} > n_{001} > n_{100}$. The birefringence of $AgTeO_2F$ is 0.078 at 1064 nm. For $Ag_2(TeO_2F_2)$, the refractive indices are in a sequence of $n_{001} > n_{010} > n_{100}$ at 1064 nm. The birefringence of $Ag_2(TeO_2F_2)$ was calculated to be 0.032 at 1064 nm, which is much smaller than that of $AgTeO_2F$. The large birefringence of $AgTeO_2F$ can be attributed to the regularly arranged TeO_3F groups.

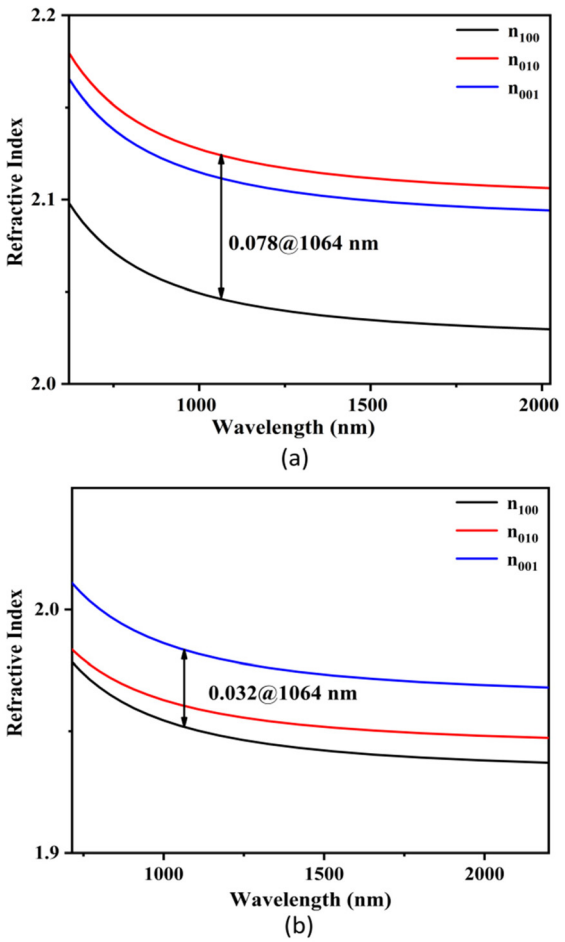

Fig. 10 Calculated refractive index dispersion curves of $AgTeO_2F$ (a) and $Ag_2(TeO_2F_2)$ (b).

Conclusions

The first cases of silver tellurite oxyfluorides, namely, $AgTeO_2F$, $Ag_2(TeO_2F_2)$ and $Ag_3F_3(TeF_6)(TeO_2)_{12}$, have been successfully synthesized through a facile hydrothermal method. $AgTeO_2F$ and $Ag_2(TeO_2F_2)$ exhibit the first examples of silver fluorotellurites and the NCS $Ag_3F_3(TeF_6)(TeO_2)_{12}$ is the first silver fluoride tellurite. The tellurite groups in these structures display three different dimensional structures, namely, 1D $[TeO_2F]_\infty$ chains in $AgTeO_2F$, 0D (TeO_2F_2) groups in $Ag_2(TeO_2F_2)$ and a 3D $[TeO_2]_\infty$ architecture in $Ag_3F_3(TeF_6)(TeO_2)_{12}$. The neutral $[TeO_2]_\infty$ open framework with 8- and 4-MPR tunnels along three crystallographic axes is first reported here. In addition, the NCS $Ag_3F_3(TeF_6)(TeO_2)_{12}$ can exhibit a moderate powder SHG effect of about 0.7 times that of commercial KDP. The birefringence of $AgTeO_2F$ was calculated to be 0.078@1064 nm, which is much larger than that of $Ag_2(TeO_2F_2)$ (0.032@1064). This work has enriched the syntheses, structures and optical properties of tellurite oxyfluorides further. Other related works about metal fluorotellurites and fluoride tellurites are underway.

Author contributions

Bo Zhang: investigation, validation and writing – original draft; Jia-Hang Wu: validation; Chun-Li Hu: formal analysis; Ya-Feng Li: validation; Fang Kong: conceptualization, supervision and writing – review and editing; Jiang-Gao Mao: supervision and funding acquisition.

Conflicts of interest

There are no conflicts to declare.

Acknowledgements

This work was supported by the National Natural Science Foundation of China (Grant No.: 91963105, 22031009 and 21921001).

References

1 C. T. Chen, Y. B. Wang, B. C. Wu, K. C. Wu, W. L. Zeng and L. H. Yu, Design and Synthesis of an Ultraviolet-Transparent Nonlinear Optical Crystal $Sr_2Be_2B_2O_7$, *Nature*, 1995, **373**, 322–324.

2 P. S. Halasyamani and K. R. Poeppelmeier, Noncentrosymmetric Oxides, *Chem. Mater.*, 1998, **10**, 2753–2769.
3 K. M. Ok, Toward the Rational Design of Novel Noncentrosymmetric Materials: Factors Influencing the Framework Structures, *Acc. Chem. Res.*, 2016, **49**, 2774–2785.
4 F. Kong, T. K. Jiang and J. G. Mao, Role of fluorine on the structure and second-harmonic-generation property of inorganic selenites and tellurites, *Chem. Commun.*, 2021, **57**, 12575–12586.
5 H. H. Cheng, W. Q. Jin, Z. H. Yang and S. L. Pan, Performance of optical materials with the derivative of planar π-conjugated groups: Recent advances and future prospects, *Inorg. Chem. Front.*, 2022, **9**, 4554–4568.
6 L. Huang and G. H. Zou, Recent Progresses of UV Nonlinear Optical Materials, *Chin. J. Struct. Chem.*, 2020, **39**, 1571–1577.
7 S. P. Guo, Y. Chi and H. G. Xue, $SnI_4{\cdot}(S_8)_2$: A Novel Adduct-Type Infrared Second-Order Nonlinear Optical Crystal, *Angew. Chem., Int. Ed.*, 2018, **57**, 11540–11543.
8 X. Huang, S. H. Yang, X. H. Li, W. Liu and S. P. Guo, Eu2P2S6: The First Rare-Earth Chalcogenophosphate Exhibiting Large Second-Harmonic Generation Response and High Laser-Induced Damage Threshold, *Angew. Chem., Int. Ed.*, 2022, **61**, e202206791.
9 X. H. Li, Z. H. Shi, M. Yang, W. Liu and S. P. Guo, Sn7Br10S2: The First Ternary Halogen-Rich Chalcohalide Exhibiting a Chiral Structure and Pronounced Nonlinear Optical Properties, *Angew. Chem., Int. Ed.*, 2022, **61**, e202115871.
10 Y. Y. Xu, C. S. Lin, D. Zhao, B. X. Li, L. L. Cao, N. Ye and M. Luo, Chemical substitution – oriented design of a new polar PbFIO3 achieving a balance between large second-harmonic generation response and wide band gap, *Scr. Mater.*, 2022, **208**, 114347.
11 W. Zeng, X. H. Dong, Y. Tian, L. Huang, H. M. Zeng, Z. E. Lin and G. H. Zou, Unprecedented boat-shaped $[Mo_2O_5(IO_3)_4]^{2-}$ polyanions induced a strong second harmonic generation response, *Chem. Commun.*, 2022, **58**, 3350–3353.
12 H. S. Ra, K. M. Ok and P. S. Halasyamani, Combining Second-Order Jahn-Teller Distorted Cations to Create Highly Efficient SHG Materials: Synthesis, Characterization, and NLO Properties of BaTeM2O9 (M = Mo6+ or W6+), *J. Am. Chem. Soc.*, 2003, **125**, 7764–7765.
13 X. L. Du, X. J. Guo, Z. L. Gao, F. A. Liu, F. F. Guo, S. Y. Wang, H. Y. Wang, Y. X. Sun and X. T. Tao, Li_2MTeO_6 (M=Ti, Sn): Mid-Infrared Nonlinear Optical Crystal with Strong Second Harmonic Generation Response and Wide Transparency Range, *Angew. Chem., Int. Ed.*, 2021, **60**, 23320–23326.
14 H. Chen, M. Y. Ran, W. B. Wei, X. T. Wu, H. Lin and Q. L. Zhu, A comprehensive review on metal chalcogenides with three-dimensional frameworks for infrared nonlinear optical applications, *Coord. Chem. Rev.*, 2022, **470**, 214706.
15 P. F. Li, C. L. Hu, F. Kong, S. M. Ying and J. G. Mao, $Y_2(Te_4O_{10})(SO_4)$: a new sulfate tellurite with a unique Te_4O_{10} polyanion and large birefringence, *Inorg. Chem. Front.*, 2021, **8**, 164–172.
16 K. C. Chen, C. S. Lin, G. Peng, Y. Chen, H. Z. Huang, E. Z. Chen, Y. X. Min, T. Yan, M. Luo and N. Ye, $LiNbTeO_5$: A High-Performance Multifunctional Crystal Material with a Very Large Second-Harmonic Generation Response and Piezoelectric Coefficient, *Chem. Mater.*, 2021, **34**, 399–404.
17 S. G. Zhao, X. X. Jiang, R. He, S. Q. Zhang, Z. H. Sun, J. H. Luo, Z. S. Lin and M. C. Hong, A combination of multiple chromophores enhances second-harmonic generation in a nonpolar noncentrosymmetric oxide: $CdTeMoO_6$, *J. Mater. Chem. C*, 2013, **1**, 2906–2912.
18 J. J. Zhang, Z. H. Zhang, Y. X. Sun, C. Q. Zhang, S. J. Zhang, Y. Liu and X. T. Tao, $MgTeMoO_6$: A neutral layered material showing strong second-harmonic generation, *J. Mater. Chem.*, 2012, **22**, 9921–9927.
19 A. Cammarata, W. G. Zhang, P. S. Halasyamani and J. M. Rondinelli, Microscopic Origins of Optical Second Harmonic Generation in Noncentrosymmetric–Nonpolar Materials, *Chem. Mater.*, 2014, **26**, 5773–5781.
20 Y. Q. Feng, H. T. Fan, Z. G. Zhong, H. W. Wang and D. F. Qiu, $Cd_3(MoO_4)(TeO_3)_2$: A Polar 3D Compound Containing d^{10}-d^0 SCALP-Effect Cations, *Inorg. Chem.*, 2016, **55**, 11987–11992.
21 Q. Wu, J. F. Zhou, X. M. Liu, X. X. Jiang, Q. X. Zhang, Z. S. Lin and M. J. Xia, $Ca_3(TeO_3)_2(MO_4)$ (M = Mo, W): Mid-Infrared Nonlinear Optical Tellurates with Ultrawide Transparency Ranges and Superhigh Laser-Induced mage ThreDasholds, *Inorg. Chem.*, 2021, **60**, 18512–18520.
22 C. Bai, Y. Chu, J. Z. Zhou, L. N. Wang, L. Luo, S. L. Pan and J. J. Li, Two new tellurite halides with cationic layers: syntheses, structures, and characterizations of CdPb2Te3O8Cl2 and Cd13Pb8Te14O42Cl14, *Inorg. Chem. Front.*, 2022, **9**, 1023–1030.
23 M. Weil and M. Shirkhanlou, Incorporation of Sulfate or Selenate Groups into Oxotellurates(IV): I. Calcium, Cadmium, and Strontium Compounds, *Z. Anorg. Allg. Chem.*, 2017, **643**, 330–339.
24 T. Wang, Y. G. Chen, Y. Guo, F. Wang, Q. Song, Y. J. Jia and X. M. Zhang, $BaLiTe_2O_5X$ (X = Cl, Br): mixed alkali/alkaline-earth metal tellurite halides with [Te2O5] infinity chains, *Dalton Trans.*, 2020, **49**, 4914–4919.
25 H. E. Lee, H. Jo, M. H. Lee and K. M. Ok, Unique synthesis, structure determination, and optical properties of seven new layered rare earth tellurite nitrates, RE(TeO3)(NO3) (RE = La, Nd, Eu, Gd, Dy, Er, and Y), *J. Alloys Compd.*, 2021, **851**, 156855.
26 K. K. Mishra, S. N. Achary, S. Chandra, T. R. Ravindran, K. K. Pandey, A. K. Tyagi and S. M. Sharma, Study of Phase Transformation in $BaTe_2O_6$ by in Situ High-Pressure X-ray Diffraction, Raman Spectroscopy, and First-Principles Calculations, *Inorg. Chem.*, 2016, **55**, 227–238.
27 J. Lin, J. Diwu, J. N. Cross, E. M. Villa and T. E. Albrecht-Schmitt, Cerium(IV) tellurite halides $[Ce_2Te_7O_{17}]X_2$ (X = Cl^-

or Br^-): the first cerium-containing cationic frameworks, *Inorg. Chem.*, 2012, **51**, 10083–10085.

28 P. F. Li, C. L. Hu, Y. P. Gong, F. Kong and J. G. Mao, $Hg_3(Te_3O_8)(SO_4)$: a new sulfate tellurite with a novel structure and large birefringence explored from d^{10} metal compounds, *Chem. Commun.*, 2021, **57**, 7039–7042.

29 B. Stöger and M. Weil, The Barium Oxotellurate(IV) Bromides $Ba_6Te_{10}O_{25}Br_2$ and $Ba_3Te_3O_8Br_2$ with Channel Structures, *Z. Anorg. Allg. Chem.*, 2012, **638**, 2150–2157.

30 W. Klein, J. Curda, E. M. Peters and M. Jansen, Neue Silber (I)-oxotellurate(IV/VI), *Z. Anorg. Allg. Chem.*, 2005, **631**, 2893–2899.

31 D. W. Lee, H. R. Noh, T. H. Kim, J. Lee, J. Y. Kim, K. T. Ko and S. H. Lim, Mixed-valent titanium tellurium oxides, Ti1_x TexTe3O8 + x (x = 0, 0.1, and 0.12): Hydrothermal synthesis, structure, and characterization, *J. Solid State Chem.*, 2021, **297**, 122024.

32 J. Chen, C. L. Hu, X. H. Zhang, B. X. Li, B. P. Yang and J. G. Mao, $CsVO_2F(IO_3)$: An Excellent SHG Material Featuring an Unprecedented 3D $[VO_2F(IO_3)]^-$ Anionic Framework, *Angew. Chem., Int. Ed.*, 2020, **59**, 5381–5384.

33 G. S. Yang, G. Peng, N. Ye, J. Y. Wang, M. Luo, T. Yan and Y. Q. Zhou, Structural Modulation of Anionic Group Architectures by Cations to Optimize SHG Effects: A Facile Route to New NLO Materials in the $ATCO_3F$ (A = K, Rb; T = Zn, Cd) Series, *Chem. Mater.*, 2015, **27**, 7520–7530.

34 Q. T. Xu and S. P. Guo, Middle-infrared Second-order Nonlinear Optical Chalcogenides and Halides Containing Multiple Anions, *Chin. J. Struct. Chem.*, 2020, **39**, 1964–1570.

35 F. G. You, P. F. Gong, F. Liang, X. X. Jiang, H. Tu, Y. Zhao, Z. G. Hu and Z. S. Lin, $M_2(SeO_3)F_2$ (M = Zn, Cd): understanding the structure directing effect of $[SeO3]2^-$ groups on constructing ordered oxyfluorides, *CrystEngComm*, 2019, **21**, 2485–2489.

36 M. L. Liang, C. L. Hu, F. Kong and J. G. Mao, $BiFSeO_3$: An Excellent SHG Material Designed by Aliovalent Substitution, *J. Am. Chem. Soc.*, 2016, **138**, 9433–9436.

37 Y. J. Jia, X. Y. Zhang, Y. G. Chen, X. X. Jiang, J. N. Song, Z. S. Lin and X. M. Zhang, $PbBi(SeO_3)_2F$ and $Pb_2Bi(SeO_3)_2Cl_3$: Coexistence of Three Kinds of Stereochemically Active Lone-Pair Cations Exhibiting Excellent Nonlinear Optical Properties, *Inorg. Chem.*, 2022, **61**, 15368–15376.

38 M. Mutailipu, M. Zhang, H. P. Wu, Z. H. Yang, Y. H. Shen, J. L. Sun and S. L. Pan, Ba3Mg3(BO3)3F3 polymorphs with reversible phase transition and high performances as ultraviolet nonlinear optical materials, *Nat. Commun.*, 2018, **9**, 3089.

39 Y. L. Hu, C. Wu, X. X. Jiang, Z. J. Wang, Z. P. Huang, Z. S. Lin, X. F. Long, M. G. Humphrey and C. Zhang, Giant Second-Harmonic Generation Response and Large Band Gap in the Partially Fluorinated Mid-Infrared Oxide $RbTeMo_2O_8F$, *J. Am. Chem. Soc.*, 2021, **143**, 12455–12459.

40 M. L. Liang, Y. X. Ma, C. L. Hu, F. Kong and J. G. Mao, Ba $(MoO_2F)_2(QO_3)_2$ (Q = Se, Te): Partial Fluorination of MoO6 Octahedra Enabling Two Polar Solids with Strong and Phase Matchable SHG Response, *Chem. Mater.*, 2020, **32**, 9688–9695.

41 J. J. Zhou, H. P. Wu, H. W. Yu, S. T. Jiang, Z. G. Hu, J. Y. Wang, Y. C. Wu and P. S. Halasyamani, $BaF_2TeF_2(OH)_2$: A UV Nonlinear Optical Fluorotellurite Material Designed by Band-Gap Engineering, *J. Am. Chem. Soc.*, 2020, **142**, 4616–4620.

42 J. Y. Chung, S. Yeon, H. Ryu, T. S. You, J. I. Jang and K. M. Ok, Nonlinear optical properties of a new polar bismuth tellurium oxide fluoride, Bi3F(TeO3)(TeO2F2)3, *J. Alloys Compd.*, 2022, **895**, 162603.

43 R. L. Tang, M. Yan, W. D. Yao, W. L. Liu and S. P. Guo, $HgTeO_2F(OH)$: A Nonlinear Optical Oxyfluoride Constructed of Active $[TeO_2F(OH)]^{2-}$ Pyramids and V-Shaped $[HgO_2]^{2-}$ Groups, *Inorg. Chem.*, 2022, **61**, 2333–2339.

44 J. H. Feng, C. L. Hu, H. P. Xia, F. Kong and J. G. Mao, $Li_7(TeO_3)_3F$: A Lithium Fluoride Tellurite with Large Second Harmonic Generation Responses and a Short Ultraviolet Cutoff Edge, *Inorg. Chem.*, 2017, **56**, 14697–14705.

45 X. X. Wang, X. B. Li, C. L. Hu, F. Kong and J. G. Mao, $Ag_4Hg(SeO_3)_2(SeO_4)$: a novel SHG material created in mixed valent selenium oxides by in situ synthesis, *Sci. China Mater.*, 2019, **62**, 1821–1830.

46 T. N. Poe, F. D. White, V. Proust, E. M. Villa and M. J. Polinski, $[Ag_2M(Te_2O_5)_2]SO_4$ (M = Ce(IV) or Th(IV)): A New Purely Inorganic d/f-Heterometallic Cationic Material, *Inorg. Chem.*, 2018, **57**, 4816–4819.

47 P. F. Li, C. L. Hu, F. Kong and J. G. Mao, $Hg_2(SeO_3)(SO_4)$: the first sulfate selenite with large birefringence explored from d10 transition metal compounds, *Mater. Chem. Front.*, 2022, **6**, 3567–3576.

48 S. N. Yan, X. X. Wang, C. L. Hu, B. X. Li, F. Kong and J. G. Mao, $Na_3Ti_3O_3(SeO_3)_4F$: A Phase-Matchable Nonlinear-Optical Crystal with Enlarged Second-Harmonic-Generation Intensity and Band Gap, *Inorg. Chem.*, 2022, **61**, 2686–2694.

49 R. H. Blessing, An Empirical Correction for Absorption Anisotropy, *Acta Crystallogr., Sect. B: Struct. Sci., Cryst. Eng. Mater.*, 1995, **A51**, 33–38.

50 G. M. Sheldrick, Crystal structure refinement with SHELXL, *Acta Crystallogr., Sect. C: Struct. Chem.*, 2015, **71**, 3–8.

51 S. K. Kurtz and T. T. Perry, A Powder Technique for the Evaluation of Nonlinear Optical Materials, *J. Appl. Phys.*, 1968, **39**, 3798–3813.

52 Y. Y. Yang, Y. Guo, B. B. Zhang, T. Wang, Y. G. Chen, X. H. Hao, X. X. Yu and X. M. Zhang, Lead Tellurite Crystals $BaPbTe_2O_6$ and $PbVTeO_5F$ with Large Nonlinear-/Linear-Optical Responses due to Active Lone Pairs and Distorted Octahedra, *Inorg. Chem.*, 2022, **61**, 1538–1545.

53 M. Zhao, Y. Sun, Y. Wu, D. Mei, S. Wen and T. Doert, NaTePO5, SrTeP2O8 and Ba2TeP2O9: Three tellurite-phosphates with large birefringence, *J. Alloys Compd.*, 2021, **854**, 157243.

54 N. Jennene Boukharrata and J. P. Laval, Synthesis and structure determination of $In_3TeO_3F_7$: An indium oxyfluorotellurate IV derived from W bronze structure with Te^{4+} in hexagonal tunnels, *J. Alloys Compd.*, 2011, **509**, 1517–1522.

55 D. D. Wang, P. F. Gong, X. Y. Zhang, Z. S. Lin, Z. G. Hu and Y. C. Wu, Centrosymmetric $Rb[Te_2O_4(OH)_5]$ and noncentrosymmetric $K_2[Te_3O_8(OH)_4]$: metal tellurates with corner and edge-sharing $(Te_4O_{18})^{12-}$ anion groups, *Inorg. Chem. Front.*, 2022, **9**, 2628–2636.

56 Y. P. Gong, Y. X. Ma, S. M. Ying, J. G. Mao and F. Kong, Two Indium Sulfate Tellurites: Centrosymmetric $In_2(SO_4)(TeO_3)(OH)_2(H_2O)$ and Non-centrosymmetric $In_3(SO_4)(TeO_3)_2F_3(H_2O)$, *Inorg. Chem.*, 2019, **58**, 11155–11163.

57 J. L. Song and C. Qian, Syntheses, Crystal Structures, and Properties of Two Quaternary Selenite/Tellurite-Nitrates with Formula of Bi(SeO3)(NO3) and Bi3(μ3-OH)(TeO3)3(NO3)2, *ChemistrySelect*, 2017, **2**, 1681–1685.

58 Y. G. Chen, N. Yang, X. N. Yao, C. B. Li, Y. Guo and X. M. Zhang, Synergetic Influence of Alkali-Metal and Lone-Pair Cations on Frameworks of Tellurites, *Inorg. Chem.*, 2018, **57**, 5406–5412.

59 S. Y. Song, D. W. Lee and K. M. Ok, Rich structural chemistry in scandium selenium/tellurium oxides: mixed-valent selenite-selenates, Sc2(SeO3)2(SeO4) and Sc2(TeO3)(SeO3)(SeO4), and ternary tellurite, Sc2(TeO3)3, *Inorg. Chem.*, 2014, **53**, 7040–7046.

60 P. F. Li, F. Kong and J. G. Mao, MII2M3IIIF3(Te6F2O16) (MII = Pb, Ba; MIII = Al, Ga): New mixed anionic tellurites with isolated Te6 coplanar rings, *J. Solid State Chem.*, 2020, **286**, 121288.

61 M. Zhao, W. M. Dong, Y. D. Wu, D. J. Mei, S. G. Wen and T. Doert, A2(TeO)P2O7 (A = K, Rb, Cs): Three new tellurite-pyrophosphates with large birefringence, *J. Alloys Compd.*, 2021, **865**, 158785.

62 Z. Li, S. Z. Zhang, W. L. Yin, Z. S. Lin, J. Y. Yao and Y. C. Wu, $Na_3Ca_4(TeO_3)(PO_4)_3$: a new noncentrosymmetric tellurite phosphate with fascinating multimember-ring architectures and intriguing nonlinear optical performance, *Dalton Trans.*, 2018, **47**, 17198–17201.

63 S. G. Zhao, Y. Yang, Y. G. Shen, B. Q. Zhao, L. N. Li, C. M. Ji, Z. Y. Wu, D. Q. Yuan, Z. S. Lin, M. C. Hong and J. H. Luo, Cooperation of Three Chromophores Generates the Water-Resistant Nitrate Nonlinear Optical Material $Bi_3TeO_6OH(NO_3)_2$, *Angew. Chem., Int. Ed.*, 2017, **56**, 540–544.

64 D. Vanderbilt, Soft self-consistent pseudopotentials in a generalized eigenvalue formalism, *Phys. Rev. B: Condens. Matter Mater. Phys.*, 1990, **41**, 7892–7895.